Photoelectrochemical Studies on Nanocrystalline Hematite Films

Ulrika Björkstén,* Jacques Moser, and Michael Grätzel

Institut de Chimie Physique, Ecole Polytechnique Fédérale, CH 1015 Lausanne, Switzerland

Received July 7, 1993. Revised Manuscript Received March 2, 1994®

Nanocrystalline hematite films supported on conducting glass have been prepared from colloidal Fe_2O_3 particles, giving a roughness factor of about 30. The current-potential characteristic showed an abnormal drop in photocurrent under reverse polarization. Photocurrent yields are low over the entire potential range. In the presence of iodide the abnormal drop was removed and the photocurrent yield increased. Action spectra were determined by illumination from the electrolyte side and the conducting glass support, respectively. The incident photon-to-current conversion efficiencies (IPCE) is a factor of 100 higher in the former compared to the latter case if water is used as a hole scavenger. In the presence of iodide this ratio is diminished 4-fold due to an increase in the IPCE value measured by illumination from the electrolyte side. The poor photocurrent yields observed are due to charge carrier recombination. Recombination at surface sites can be partially intercepted by adsorbed iodide.

Introduction

Hematite is an attractive semiconductor material to consider for photoelectrochemical investigations. It shows good stability, and its bandgap of 2.2 eV gives an absorption spectrum that reaches far out in the visible. The level of the valence band edge (+1.6 V/SCE at pH 14)[1] also makes it suitable for photoinduced oxygen evolution from water. Because of these favorable characteristics, several authors have previously investigated the possibilities of using hematite for solar energy conversion. In general, however, it was concluded that the recombination losses in the solid were too great for any practical application, because of the short diffusion length of the minority carriers; Kennedy et al. determined Lp to 2-4 nm only.[2] Accordingly, Bockris et al.[3] found that a stack of ten 60-nm-thick photoelectrodes gave a current 3 times that obtained by one electrode of thickness 600 nm. Measurements done earlier in our laboratory[9] also showed a high quantum yield in photoinduced oxidation of iodide on 120-nm-sized iron oxide colloids in suspension in a strongly acidic environment.

Our approach was then to prepare an Fe_2O_3 film with a nanocrystalline morphology of the kind already well established for TiO_2.[4] Since in such systems the distance the hole has to diffuse before reaching the interface is only a few nanometers, the minority carriers can be rapidly captured by the electrolyte present in the nanopores. This should lead to diminished recombination losses in the bulk. Here we present our first observations with this type of nanostructured hematite films.

Experimental Section

Electrode Preparation. Colloidal Fe_2O_3 was prepared by hydrolysis of ferric trichloride. $FeCl_3$ (50 g) was dissolved in 100 mL of 0.1 M HCl. H_2O (500 mL) was heated to boiling in an Erlenmeyer flask, and the solution of $FeCl_3$ was then added dropwise under vigorous stirring. Incubation for an hour, under continuous stirring, was followed by dialysis of the suspension during 24 h using a Visking dialysis tube of cellulose with a pore size of 2-5 nm. The exterior water was changed a total of six times. Colloidal particles with an average radius of 10 nm were obtained, as determined by light-scattering measurement. The suspension was then concentrated using a rotary evaporator to about 100 g/L. Triton-X (100), a non-ionic surfactant, was added in the quantity 1 drop/mL colloidal suspension in order to prevent aggregation and to help wetting of the conducting glass on which the suspension was deposited. The conducting glass was prepared by spray pyrolysis. A solution of $SnCl_4$ and NH_4F in ethanol was sprayed onto a microscope slide at 450 °C to yield a 0.5-μm-thick layer of fluor-doped (0.5%) SnO_2. The Fe_2O_3 colloidal suspension was deposited on the SnO_2 layer using a Pasteur pipet. Thereafter, the electrode was dried for at least 1 h at room temperature before sintering in a Solo (111-7/5/18) oven at 560 °C for 4 h.

Structural Characterization of the Films. The structure of the film was determined by scanning electron microscopy, and the results are shown in Figure 1. The cross section of the film was examined in two different magnifications. It consists of particles with diameters between 25 and 75 nm sintered together to form a nanoporous structure. The thickness of the iron oxide layer is 1-1.5 μm. Thicker layers than this cracked. The roughness factor of the electrode was estimated by immersing a 1.5 cm^2 sized electrode in 10 mL of a 10^{-4} M solution of $K_3Fe(CN)_6$ in ethanol for 3 days. The absorption spectrum of the solution was then compared with that of the fresh solution to determine the decrease in concentration and the number of molecules that had thus been adsorbed onto the iron oxide surface. The number of molecules adsorbed was in this way calculated to be 9×10^{15}. The surface occupied by one molecule was taken to be 50 $Å^2$, and the total area covered was thus 45 cm^2. Dividing this by the geometric area gives a roughness factor of 30, which seems reasonable compared to what has already been obtained for electrodes of this type of structure.[4] Moreover, calculating the average surface area of one colloidal particle to 7.8×10^{-15} m^2 and the number of particles to 1.2×10^{12} in a 1-μm-thick electrode with a geometric area of 1.5 cm^2, we obtain a total iron oxide surface area of 94 cm^2. If we assume 50% of this area to be exposed to the adsorbent the interface will be 47 cm^2, which gives a roughness factor of 31.

X-ray diffraction measurements gave a diffraction pattern showing hematite superimposed on cassiterite (SnO_2) for the sintered electrode, whereas the unsintered electrode showed only the diffraction pattern of cassiterite. This indicates either that the crystallization takes place during sintering, the colloidal

® Abstract published in *Advance ACS Abstracts*, April 1, 1994.

(1) Dare-Edwards, M. P.; Goodenough, J. B.; Hamnett, A.; Trevelick, P. R. *J. Chem. Soc., Faraday Trans. 1* **1983**, *79*, 2027-2041.
(2) Kennedy, J. H.; Frese, K. W., Jr. *J. Electrochem. Soc.* **1978**, *125*, 109.
(3) Itoh, K.; Bockris, J. O'M. *J. Appl. Phys.* **1984**, *56* (3), 874.
(4) O'Regan, B.; Moser, J.; Anderson, M.; Grätzel, M. *J. Phys. Chem.* **1990**, *94*, 8720.
(5) Kennedy, J. H.; Shinar, R.; Ziegler, J. D. *J. Electrochem. Soc.* **1980**, *127*, 2307.
(6) Hagfeldt, A.; Björkstén, U.; Lindquist, S.-E. *Sol. Energy Mater. Sol. Cells* **1992**, *27*, 2993-304.

0897-4756/94/2806-0858$04.50/0

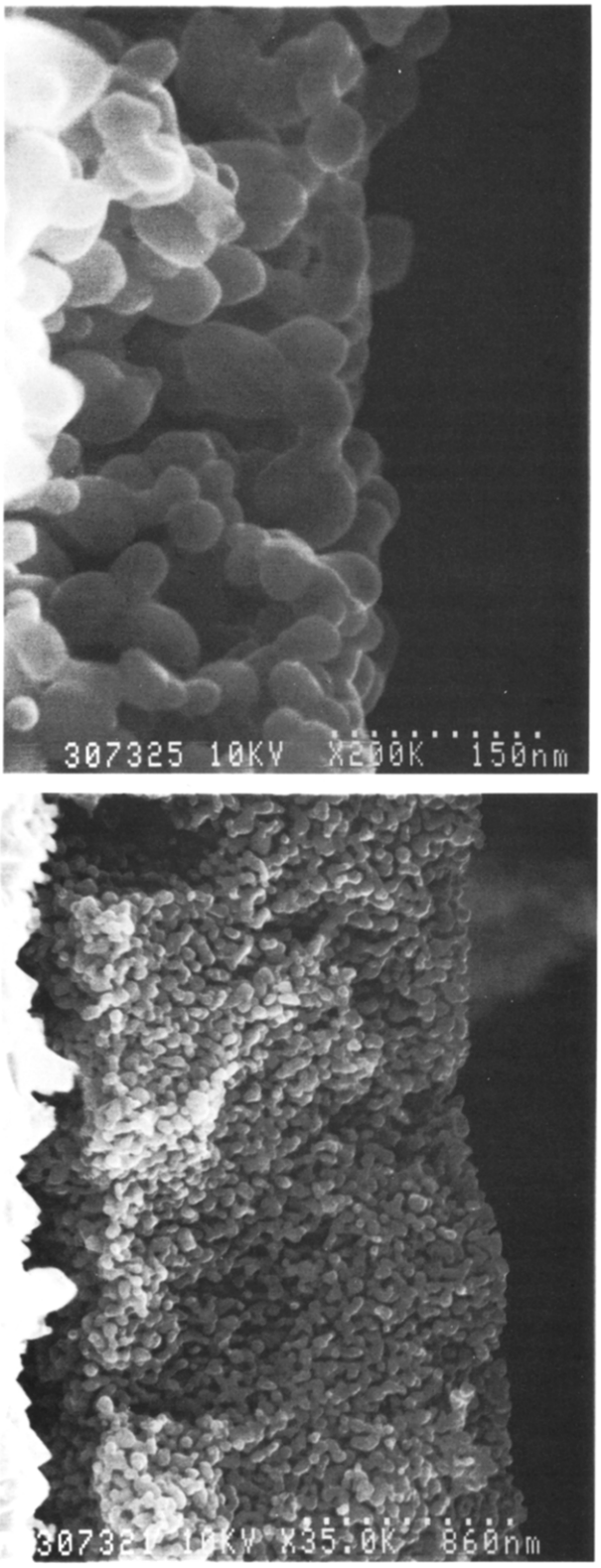

Figure 1. Scanning electron micrograph of the edge of the porous electrode at two different magnifications; sintered nm size hematite particles on a conducting cassiterite (SnO_2) support; (a, top) magnification 37 000 times; (b, bottom) magnification 5 800 times.

particles being initially amorphous, or that the isolated unsintered crystallites are too small to give rise to a diffraction pattern. The important information derived from these measurements is that the sintered electrode consists of hematite and that no other iron oxide crystalline phase can be detected. The mean crystallite size calculated from the peak widths of the diffraction spectra was 50 nm, in agreement with the SEM results.

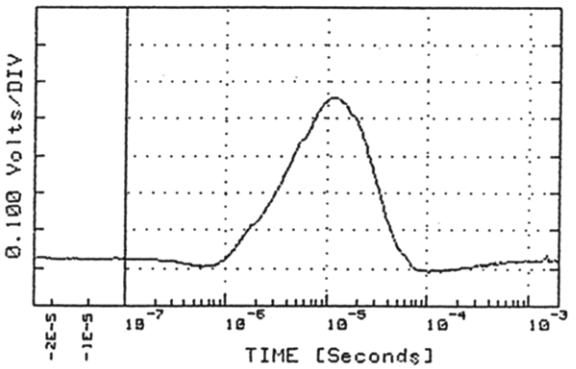

Figure 2. Transient current signal following the nanosecond laser pulse, displayed on a logarithmic time scale. The electrolyte was 50 mM KI in 0.1 mM NaOH (aq), and the potential was 500 mV/SCE. The current is converted to a voltage with a sensitivity of 5 mA/V, so the maximum current corresponds to 0.45 mA, and the total charge is 26 nC. The 532-nm laser pulse had a total energy of 10 mJ.

Spectroscopic Measurement of the Flat-Band Potential. The flat-band potential was estimated by spectroscopic probing of the Burstein shift at different potentials. A spectroelectrochemical cell was used where the transparent Fe_2O_3 working electrode formed a window, and the Ag/AgCl reference electrode as well as the Pt counter electrode were outside the analyzing beam of the Hewlett-Packard 8450A spectrophotometer. As electrolyte was used 0.1 M $LiClO_4$(aq), and the pH was adjusted using $HClO_4$. This electrolyte was chosen because of its inertness. The same potentiostat as for the photocurrent measurements was used. This method has been described in detail by Redmond et al.,[7] who applied it to ZnO electrodes fabricated in a similar way.

Mott–Schottky plots to estimate the flat-band potential in NaOH and LiI were measured using an Autolab potentiostat applying an ac voltage amplitude of 10 mV and scanning the dc voltage between −1 and +1 V. Measurements were done at frequencies between 10 and 1000 Hz.

Photocurrent–Potential Measurements. All measurements employed a standard three-electrode system with SCE as a reference, and a platinum grid counter electrode. The working electrode was illuminated through the electrolyte–iron oxide interface. The electrodes were dipped in a polystyrene beaker containing the electrolyte. A Pine Instruments RDE 3 potentiostat was used for potentiostatic control. All potentials reported are versus SCE. Preliminary steady-state illumination experiments carried out with simulated AM 1.5 sunlight gave a low anodic photocurrent (a few microamperes) superimposed on a dark current that quickly became anodically large at potentials positive of 400 mV/SCE. To quantitatively study the effect of potential on the photocurrent, we chose to measure the transient photocurrent that followed upon exciting the film with a nanosecond, frequency-doubled (532 nm), 10-mJ Nd:YAG laser pulse. The current output of the potentiostat was fed to either of two different types of Tektronix acquisition systems, a DSA 602 A digitizing signal analyzer, and a system based on the 7612 D programmable digitizer. The time-resolved photocurrent curve was obtained in this way (Figure 2). Integrating the current over time yields the total charge collected as a result of the laser excitation.

Action Spectra. Photoinduced charge separation and carrier transport in the nanocrystalline hematite film was further investigated by measuring action spectra under different conditions. The electrochemical setup was the same as in the previous section, the potential being fixed at 400 mV/SCE. The light source was an Oriel 450-W xenon lamp chopped at a frequency of 3 Hz. The chopper signal was fed to the reference channel of an EG&G 5206 two-phase lock-in analyzer, and the output from the potentiostat was connected to the signal channel so that the in-phase photocurrent could be detected. An Oriel 77250

(7) Redmond, G.; O'Keefe, A.; Burgess, C.; MacHale, C.; Fitzmaurice, D. *J. Phys. Chem.*, in press.

monochromator was used, and the incident monochromatic light power was measured with a YSI-Kettering 65A radiometer. The working electrode was illuminated either through the electrolyte/electrode (Fe_2O_3) interface (EE) or through the substrate (SnO_2)/electrode interface (SE). For SE illumination the absorption of light by the substrate (glass and SnO_2 layer) has been taken into account in calculating the incident photon-to-current conversion efficiency (IPCE).

Dark Currents. The same three-electrode system was used to measure dark currents. An EG&G Model 362 scanning potentiostat with a scanning rate of 5 mV/s was used. Measurements were done at pH 12.4 in two aqueous electrolytes: 0.1 M $NaClO_4$ with 15 mM NaOH, and the same electrolyte with 20 mM LiI added to the solution. The area of the Fe_2O_3 electrode was 2 cm^2.

Results and Discussion

The spectroscopic measurement on the Fe_2O_3 electrode gave an estimated flat-band potential of −550 mV/SCE at pH 10.7 and +50 mV at pH 2.7, the difference of 600 mV being about 100 mV larger than what would be expected from a Nernstian shift. Mott–Schottky plots showed frequency dispersion and bad linearity. The flat-band potential measured with this method could however be estimated to −650 mV at pH 12 (10 mM NaOH), and no significant shift or change in the form of the plot could be detected adding 0.1 M LiI to the electrolyte. While this supports the notion that I^- is not a potential determining ion for Fe_2O_3, these measurements should be interpreted with caution. Due to the nanocrystalline morphology of the film affecting depletion layer formation, the simple Mott–Schottky equation may not be applicable. Detailed analysis of the impedance behavior of nanocrystalline oxide semiconductor films is presently under way.

The dark current had an anodic onset at 600 mV/SCE without the presence of iodide and had at 800 mV reached 0.6 mA (Figure 4c). With iodide added to the solution the onset was moved to 450 mV/SCE, and at 800 mV the dark current was 1 mA. This is more than 10 times as large as the dark current measured from the bare tin oxide support in the same electrolytes.

Figure 3a shows the effect of potential on the magnitude of the charge collected after laser excitation of the hematite film. In aqueous 0.1 M NaOH, the photoresponse has an onset at about −700 mV, near the expected level of the flat-band potential at pH 13. It augments steadily with increasing reverse bias until a sudden drop occurs between 500 and 600 mV. In 0.5 M KI(aq) as electrolyte the drop in photocurrent is no longer observed. The onset moves some 200 mV in the positive direction in accordance with a Nernstian shift of the flat-band potential due to the change in pH. Increasing the pH from 7.6 to 13.1 by addition of 0.1 M NaOH displaces the photocurrent onset back to the value of −700 mV observed for pure NaOH. Interestingly, the drop in photocurrent at 500 mV does not reappear in the presence of iodide. Apparently, iodide affects the behavior of the photocurrent at positive potentials. The extent to which this effect occurs is controlled by the relative concentration of OH^- and I^- at the Fe_2O_3 surface. To investigate this matter the photocurrent potential curve was measured using 0.05 M KI, and varying the NaOH concentration from 0 to 0.1 M (Figure 3b). If the iodide concentration is an order of magnitude greater than the hydroxyl concentration, then the drop in photocurrent is suppressed. In contrast, if the iodide concentration is one order of magnitude smaller than the hydroxyl concentration, the effect of iodide vanishes altogether. This indicates that the surface

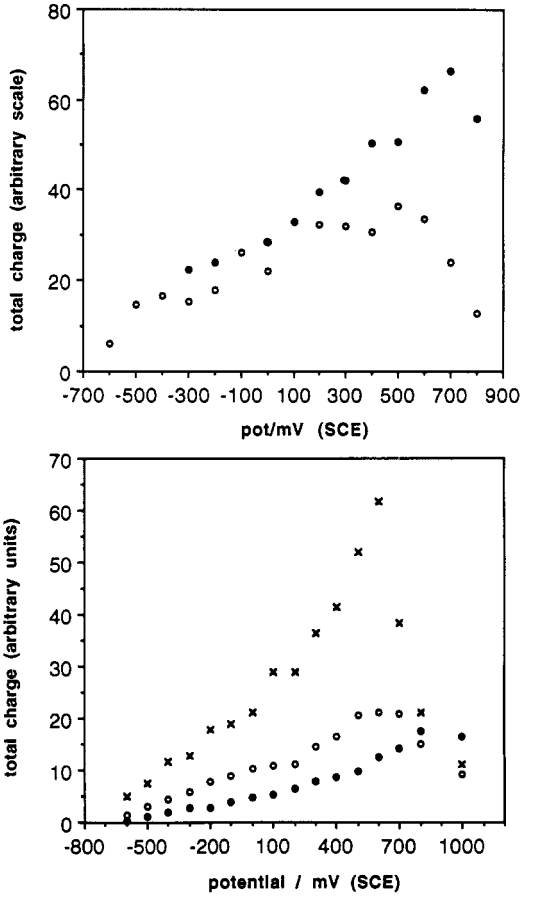

Figure 3. Total charge (normalized scale) passing through the circuit as a transient current following the laser pulse irradiation. Effect of iodide on the *IV* characteristic: (a, top) open circles 0.1 M NaOH (aq), filled circles 0.1 M NaOH and 0.5 M KI (aq); (b, bottom) filled circles 50 mM KI (aq), open circles 50 mM KI and 10 mM NaOH (aq), crosses 50 mM KI and 0.1 M NaOH (aq). (The characteristics obtained using 50 mM KI with 1 or 0.1 mM NaOH were identical with the result obtained using only 50 mM KI.)

adsorption of iodide, competing with the adsorption of hydroxyl groups, is indeed responsible for the elimination of the drop in photocurrent at positive potentials.

A likely explanation for this phenomenon is the presence of surface states, whose energetic position is estimated to be centered at about 550 mV/SCE. When the semiconductor is polarized positive with respect to this potential, the surface states are empty and could become efficient recombination centers via trapping of conduction band electrons. Iodide could fill these traps by electron donation, rendering them ineffective. The effect of iodide on the anodic dark current giving an earlier onset and higher values can only be explained by oxidation of iodide by bandgap states. Our Mott–Schottky plots (Figure 4) show a sudden increase in capacitance at 600 mV/SCE, implying the addition of a capacitance parallel to the depletion layer capacitance at this potential. Our interpretation is that this is due to the partial emptying of the mentioned surface states. Goodenough et al.[1] also deduced from capacitance measurements the presence of surface states at 0.7 V/SSE in 1 M KOH. The surface states were removed by adding quinol to the solution, and the authors believe this effect to be due to quinol stabilizing Fe^{3+}. Kennedy et al.[5] observed a photocurrent increase after dipping a polycrystalline sintered Fe_2O_3 electrode in KI solution in agreement with our observations.

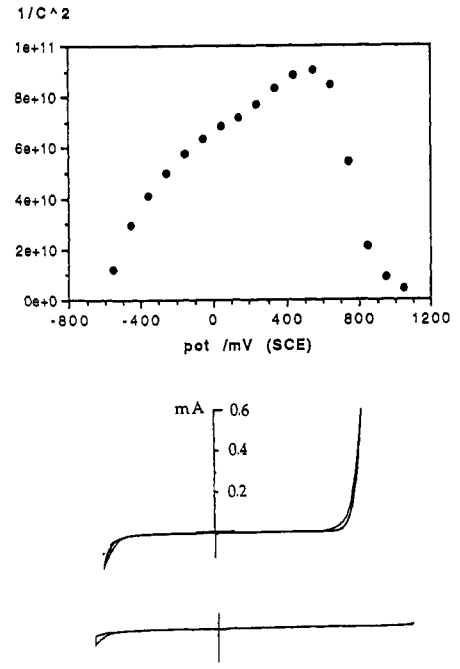

Figure 4. Mott–Schottky plot of the hematite electrode (top) obtained at 1000 Hz using 10 mM NaOH (aq) as electrolyte, with the dark current at corresponding potentials showed underneath. The dark current was measured in 0.1 M $NaClO_4$ and 15 mM NaOH (aq). The third graph (bottom) shows the dark current in the same electrolyte when the hematite electrode has been replaced by a bare tin oxide support. The area of the electrode was 2 cm^2.

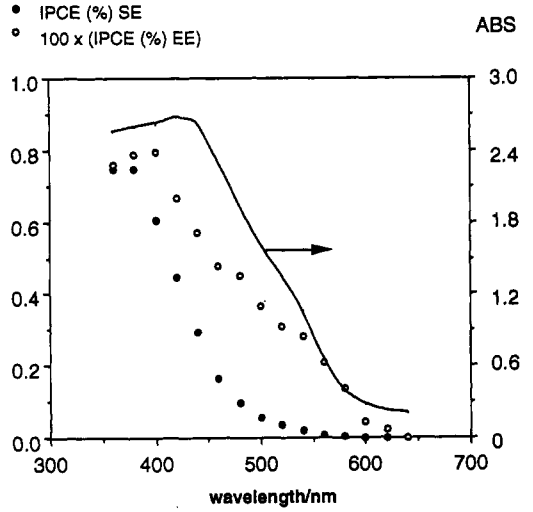

Figure 5. Absorption spectrum of the hematite electrode (reference: SnO_2-covered glass and action spectra obtained when illuminating the electrode through the substrate (SE) and directly onto the interface with the electrolyte (EE). Note that the scale of the IPCE values differs with a factor of 100 in the two cases. Electrolyte: 0.1 M NaOH (aq).

Figure 5 shows the features of the action spectrum for both SE and EE type illumination as well as the absorption spectrum of the Fe_2O_3 film. The IPCE for the EE direction is however 2 orders of magnitude smaller than that for SE. There is also a red shift in the action spectrum. The pronounced difference in IPCE values under EE and SE illumination shows that the collection of photogenerated electrons across the hematite film is very inefficient. Charge carriers produced in the vicinity of the conducting glass back contact are collected more efficiently, but the low IPCE values even on SE illumination contrasts the behavior of nanocrystalline TiO_2 films where photoinduced charge separation as well as charge transport across electrodes of thicknesses between 0.5 and 7 μm is efficient.[6] For the porous TiO_2 electrode the IPCE maxima obtained on SE illumination range between 10% and 65%, depending on the electrode thickness. As the lowest IPCE (SE) values in this case were obtained for the thickest electrode (7 μm), where diffusion of the hole scavenger to inner colloidal layers may be expected to be slow, a limiting factor to the charge collection seems to be the hole transfer to the electrolyte. The low photocurrent yields obtained on the Fe_2O_3 electrodes could hence be due to a combination of a short hole diffusion length and the crystallite size which is slightly larger in the Fe_2O_3 than in the TiO_2 films. In the case of Fe_2O_3, the minority carriers have to diffuse over a larger distance before reaching the surface where they are scavenged. Given the small hole diffusion length of 2–4 nm in hematite, it is not surprising that charge carrier recombination is still dominant in the present films having a particle size in the 25–75-nm range. The diameter of the nanocrystals would have to be decreased to 5–10 nm in order to render interception of the recombination by hole scavenging at the surface effective. Although we have prepared Fe_2O_3 colloids of this size, investigations of films formed by these very small particles have been hampered so far by adhesion problems. To get a film that adheres well to the substrate, sintering time and temperature are such that particle growth takes place during the sintering process.

The observed red shift of the EE action spectrum is consistent with a limited charge transport through the electrode. Shorter wavelengths are absorbed by the outer colloidal layers, whereas longer wavelengths with a lower absorption coefficient will penetrate further into the electrode and be absorbed by colloidal layers closer to the back contact. This red shift is smaller than what was generally observed for the TiO_2 electrodes and by Hodes et al.[8] for electrodeposited, porous CdS electrodes, in a similar study. In these two cases the IPCE(EE) values actually come to a maximum and decrease again toward shorter wavelengths. This maximum cannot be observed in the action spectra of the Fe_2O_3 electrodes. It should be pointed out that there are two types of optical transitions in Fe_2O_3. The first is of d–d character and is mainly located in the visible while the second corresponds to the 3-eV absorption edge due to transitions between occupied 2p orbitals of O^{2-} and the unoccupied d orbitals of Fe^{3+} forming the conduction band. The photocurrent action spectrum obtained with Fe_2O_3 does not match the absorption in the visible, indicating a lower charge carrier generation quantum yield in the visible as compared to UV light. This could mask the feature of a photocurrent maximum which is expected for a wavelength-independent quantum yield for charge carrier generation. However, an action spectrum of the TiO_2 electrode measured at very low pH follows the same pattern as what was generally seen for the Fe_2O_3 electrode. The charge collection efficiency is significantly lower on EE than on SE illumination, but there is only a small red shift. Two current limiting factors are present: Especially in the absence of hole traps, bulk hole–electron recombination within the colloids on one hand will favor charge separation

(8) Hodes, G.; Howell, I. D. J.; Peter, L. M. *J. Electrochem. Soc.* **1992**, *139* (11), 3136.
(9) Moser, J.; Grätzel, M. *Helv. Chim. Acta* **1982**, *65*, 1436.

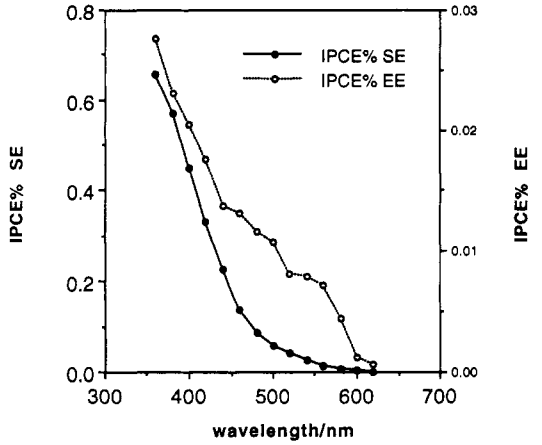

Figure 6. Action spectra obtained in 0.1 M NaOH and 0.1 M LiI (aq).

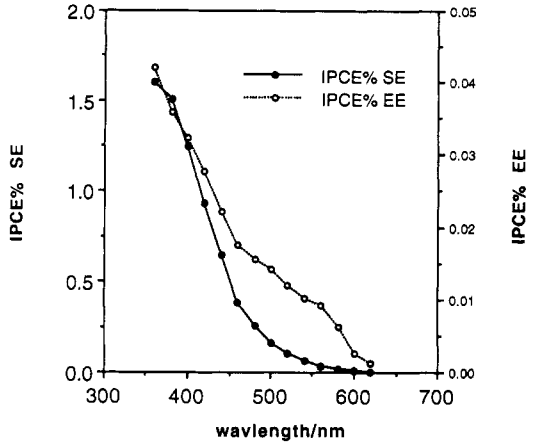

Figure 7. Action spectra obtained in 0.1 M LiI (EtOH).

at outer colloidal layers (shorter wavelengths on EE-illumination). On the other hand, grain boundary and surface recombination (possibly with surface-trapped holes) limits the transport of electrons through the electrode to the back contact, favoring charge separation at inner colloidal layers (longer wavelengths on EE illumination). The relative importance of the different mechanisms of recombination might determine the red shift of the EE action spectrum, and the relative IPCE-(SE/EE) values. Looking closer at the results of Hodes et al., we observe that the photocurrent maximum of the EE action spectra is less pronounced on CdS films deposited at higher temperatures. Particle growth at higher deposition temperatures may lead to less efficient hole transfer from the bulk of the colloids to the interface with the electrolyte. Moreover, films with larger particles contain fewer grain boundaries per unit distance which could possibly lead to a decrease in grain boundary recombination.

To further discriminate between the different recombination mechanisms in our present study, action spectra using the following three different electrolytes were measured: 0.1 M NaOH (aq), 0.1 M NaOH + 0.1 M LiI (aq), and 0.1 M LiI (EtOH). Comparing Figure 6 with Figure 5, one sees that adding iodide to the electrolyte increases the IPCE(EE) 3-fold, whereas on the IPCE(SE) there is no effect at short wavelengths. For wavelengths above 500 nm the increase in photocurrent is however important also for SE type excitation. These wavelengths penetrate further into the Fe_2O_3 and will hence be absorbed by outer colloidal layers rendering the effect of iodide similar to that observed for EE illumination. Iodide can affect only surface recombination. It affects the role of surface states and traps holes more efficiently than water. While the improvement in the yield is marked especially for EE type excitation, the IPCE values remains below 1% even in the presence of iodide, indicating that bulk or grain boundary recombination is dominant. This is further confirmed by results obtained with solution of iodide in ethanol (Figure 7). With regards to aqueous iodide electrolyte, the increase in IPCE(SE) is a factor of 2, while it is only 30% for IPCE(EE). Better diffusion of iodide into the pores of the electrode can be expected because of lower surface tension in ethanol, rendering hole transfer especially from inner colloidal layers more efficient, hence giving rise to the observed increase in IPCE(SE). Ethanol may in itself also serve as a hole scavenger which would give the same result.

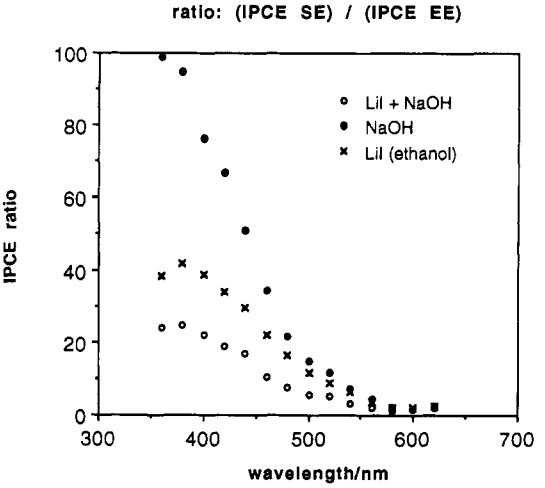

Figure 8. Ratio of the IPCE values obtained on SE and EE illumination for the three different electrolytes.

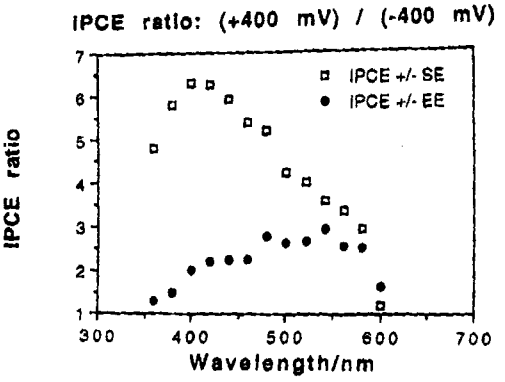

Figure 9. Ratio of the IPCE values obtained on SE and EE illumination at two different potentials: +400 mV/SCE and −400 mV/SCE.

Figure 8 compares the ratio of the action spectra for front and back side excitation obtained under the different conditions. With 0.1 M NaOH the IPCE ratio is large with a maximum of 100. Adding 0.1 M LiI increases the IPCE(EE). This brings down the IPCE(SE/EE) ratio to a maximum of about 20. Replacing water by ethanol increases the IPCE(SE) augmenting again the IPCE(SE/EE) ratio to a maximum of about 40. In all cases the (SE/EE) ratio is smaller for longer wavelengths. This is plausible in view of the longer penetration length of the light.

Figure 9 shows the ratio of the IPCE's at two different potentials. The collection efficiency of charge carriers

created close to the back contact is most sensitive to the potential applied. The further away from the back contact, the smaller is the effect of the applied potential. This indicates that the potential drop takes place across the colloidal layers closest to the back contact and that the outer layers are hardly affected at all, but stay at the equilibrium potential.

Conclusion

Nanocrystalline Fe_2O_3 films have been prepared and their photoelectrochemical behavior has been investigated. The use of a conducting glass support for the film has allowed us to determine incident photon to current conversion efficiencies under front and back side light excitation. The strikingly large difference in yields observed indicates that charge carrier recombination is the controlling factor for the photocurrent. By scrutinizing the effect of iodide on the performance of the electrode the influence of surface phenomena has been unraveled. Even in the presence of such hole scavengers the photocurrent yields remain small, the highest value obtained being 1.7%. The reason for this is that bulk and/or grain boundary recombination of charge carriers remains dominant even for Fe_2O_3 films constituted of particles in the 25–75-nm size range. The higher quantum yields obtained on colloids in suspension points at grain boundary recombination in the electrodes.

Acknowledgment. We gratefully acknowledge the excellent collaboration of Dr. V. Shklover at the Federal Institute of Technology in Zürich, who produced the micrographs and X-ray diffractograms of the electrodes.